J Solid State Electrochem (2012) 16:1271–1277
DOI 10.1007/s10008-011-1523-4

ORIGINAL PAPER

Oleic acid-assisted preparation of $LiMnPO_4$ and its improved electrochemical performance by Co doping

Zhao Yang · Gao-Shao Cao · Jian Xie · Xin-Bing Zhao

Received: 24 May 2011 / Revised: 31 July 2011 / Accepted: 2 August 2011 / Published online: 17 August 2011

Abstract $LiMnPO_4$, with a particle size of 50–150 nm, was prepared by oleic acid-assisted solid-state reaction. The materials were characterized by X-ray diffraction, field emission scanning electron microscopy, and transmission electron microscopy. The electrochemical properties of the materials were investigated by galvanostatic cycling. It was found that the introduction of oleic acid in the precursor led to smaller particle size and more homogeneous size distribution in the final products, resulting in improved electrochemical performance. The electrochemical performance of the sample could be further enhanced by Co doping. The mechanism for the improvement of the electrochemical performance was investigated by Li-ion chemical diffusion coefficient $\left(\widetilde{D}_{\mathrm{Li}}\right)$ and electrochemical impedance spectroscopy measurements. The results revealed that the $\widetilde{D}_{\mathrm{Li}}$ values of $LiMnPO_4$ measured by cyclic voltammetry method increase from 9.2×10^{-18} to 3.0×10^{-17} cm^2 s^{-1} after Co doping, while the charge transfer resistance (R_{ct}) can be decreased by Co doping.

Keywords $LiMnPO_4$ · Oleic acid · Co doping · Li-ion batteries · Electrochemical performance

Introduction

Li-ion batteries (LIBs) [1] are now the dominant power sources for portable electronic equipment, such as mobile phones, digital cameras, and laptop computers, due to their high voltage, high energy density, and long cycle life. LIBs also show potential applications in electric vehicles (EV) and hybrid electric vehicles (HEV) [2–4]. The currently used $LiCoO_2$ cathode material [5–7], however, is not appropriate for a large-scale application, such as in EV and HEV, due to its high cost and toxicity. Therefore, the development of cheap, eco-friendly, and safe cathode materials becomes extremely important.

Among various cathode materials, the olivine-type $LiMPO_4$ (M=Fe, Mn, Co, Ni) materials [8–11] are the most promising because of their stable structure and high safety, environmental friendliness, and high theoretical capacity (170 mAh g^{-1}). In the olivine family, $LiFePO_4$ has received special interest owing to its easy preparation and excellent electrochemical performance [4, 12–14]. However, its intrinsically low working voltage (3.4 V vs. Li/Li^+) and low density may limit its practical application. Although $LiCoPO_4$ and $LiNiPO_4$ exhibit high working voltages (4.8 and 5.1 V, respectively), they suffer from rapid capacity fade [15–17]. In addition, the electrolyte may become unstable at such a high voltage. In this regard, $LiMnPO_4$ seems to be a better choice because it gives a reasonable working voltage of 4.1 V and a high energy density of 684 Wh kg^{-1}. Unfortunately, this material shows extremely low ionic and electronic conductivities [18–20], which make its practical capacity far below 170 mAh g^{-1}. So far, the effective methods to improve the electrochemical performance of $LiMnPO_4$ include Mn-site doping [21–23], particle size minimizing [18, 24, 25], and carbon coating [26–28]. As reported by Lee et al. [20], Mg and Zr dually doped $LiMnPO_4$ displayed a superior electrochemical performance than the undoped one. The electrochemical performance of $LiMnPO_4$ at high current densities, however, is not satisfactory yet.

Z. Yang · G.-S. Cao · J. Xie · X.-B. Zhao (✉)
Department of Materials Science and Engineering,
Zhejiang University,
Hangzhou 310027, China
e-mail: zhaoxb@zju.edu.cn

It is generally accepted that particle size minimizing is indispensable to improve the electrochemical performance of $LiMnPO_4$. It is, however, difficult to prepare nanosized $LiMnPO_4$ by high-temperature solid-state reaction. In this work, nanosized $LiMnPO_4$ was successfully prepared by oleic acid-assisted solid-state reaction. The effect of adding oleic acid during ball milling on the microstructure and electrochemical performance of final products was investigated. Co doping was used to further improve the electrochemical performance. Li-ion diffusion coefficients and electrochemical impedance spectroscopy (EIS) measurements were used to understand the effect of Co doping on the electrochemical behavior of the samples.

Experimental

$LiMnPO_4$ (or Co-doped $LiMnPO_4$) was prepared via solid-state reaction using $Li(CH_3COO)\cdot 2H_2O$, $Mn(CH_3COO)_2\cdot 4H_2O$, $Co(CH_3COO)_2\cdot 4H_2O$, and $NH_4H_2PO_4$ as the starting materials. The starting materials, with a Li/(Mn+Co)/P molar ratio of 1.02:1:1 (with a total weight of about 23.4 g), were sufficiently mixed by ball milling at 400 rpm for 10 h using acetone (50 mL) as the milling media and oleic acid (5 mL) as the surfactant. The resulting mixture was dried at 60 °C for 12 h to get the precursor. The precursor was heated at 400 °C for 5 h under N_2 followed by ball milling again at 400 rpm for 6 h. After drying, the powder was heated at different temperatures (550, 600, and 650 °C) for 5 h under N_2. The sample was named as LMP-1-*T*, where *T* is referred to as the heating temperature. For comparison, a similar process was used to prepare $LiMnPO_4$ using the precursor without oleic acid treatment. The sample was named as LMP-2-*T*. The Co-doped sample, $LiMn_{0.95}Co_{0.05}PO_4$, was named as LMP-3-*T*.

The crystal structure of the samples was examined by X-ray diffraction (XRD) using Cu K_α radiation (λ=0.154 nm) on a Rigaku D/Max-2550pc powder diffractometer. The morphologies of the samples were observed by field-emission scanning electron microscopy on a FEI-sirion microscope and transmission electron microscopy (TEM) on a JEM 2100F microscope. The carbon content was measured on a Flash EA-1112 tester.

The electrochemical performance of the $LiMnPO_4$ (or $LiMn_{0.95}Co_{0.05}PO_4$) was evaluated using CR2025-type coin cells. The electrode slurry was made by mixing 70 wt.% active material, 20 wt.% acetylene black, and 10 wt.% polyvinylidene fluoride in *N*-methyl pyrrolidone with magnetic stirring for 2 h. The slurry was then pasted onto aluminum foil to make the working electrodes. After drying at 80 °C in air, the electrodes were pressed at a pressure of 10 MPa. The electrodes were assembled into half cells in an argon-filled glove box using metallic Li foil as the counter-electrode, 1 M $LiPF_6$ in ethylene carbonate/dimethyl carbonate (1:1 by volume) as the electrolyte, and polypropylene microporous film (Celgard 2300) as the separator. Galvanostatic cycling test was conducted between 2.5 and 4.5 V at 1/20 to 1 C (1 C=140 mA g^{-1}) rates on a Lisun PCBT-100-64D battery tester. The regime for galvanostatic cycling is that the cells were charged at a constant current to 4.5 V and kept at 4.5 V for 1 h, followed by discharge at a constant current to 2.5 V. A previous work by Wang et al. [16] showed that this electrolyte is stable up to 5.1 V. Cyclic voltammetry (CV) measurements were conducted between 2.5 and 5 V at scan rates from 0.1 to 2.0 mV s^{-1} on an Arbin-001 MITS 2.9-BT2000. EIS measurements were carried out on a CHI660C electrochemistry workstation. The impedance plots were recorded by applying an AC signal of 5-mV amplitude over the frequency range from 10^5 Hz to 10 mHz at de-lithiation state. All of the electrochemical measurements were performed at room temperature.

Results and discussion

Figure 1 compares the SEM images of precursors with and without the introduction of oleic acid during ball milling. The precursor with oleic acid treatment is composed of well-dispersed nanoparticles with a size of 50–150 nm. The particles exhibit a smooth surface and a uniform size distribution. Without the treating by oleic acid, on the contrary, the particles tend to aggregate. In addition, the particles also show a rough surface and a wide size distribution. It is obvious that the introduced oleic acid plays an important role in the morphology of the precursors, which in turn will have influence on the morphology of the final products. During ball milling in acetone, the hydrophilic group (−COOH) in oleic acid tends to adsorb on the surface of the precursor particles, while the oleophillic group ($-(CH_2)_7CH{=}CH(CH_2)_7CH_3$) tends to stretch into the acetone [18], resulting in the formation of a unique structure: particles in oleic acid. Such a structure can prevent the precursor particles from growing and aggregating.

Figure 2 shows the XRD patterns of the samples prepared at different temperatures. All diffraction peaks of the samples can be indexed to orthorhombic $LiMnPO_4$ with a space group of *Pnmb* (JCPDS card no. 72–0426) without the formation of any impurities. No diffraction peaks related to carbon can be detected, indicating its amorphous nature.

Figure 3 compares the SEM images of the final product $LiMnPO_4$. For sample LMP-1-400, it consists of particles of 50–100 nm in size with a relatively uniform size distribution as seen in Fig. 3a. The particles show slight

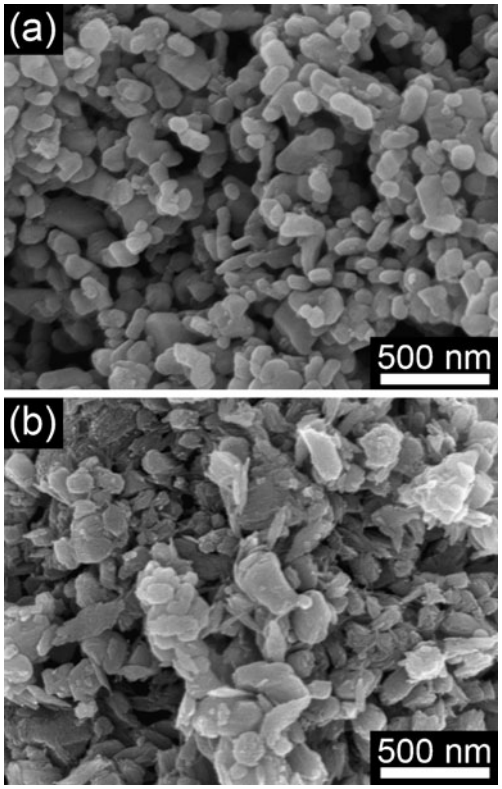

Fig. 1 SEM images of precursors **a** with and **b** without the introduction of oleic acid during ball milling

growth and aggregation after the secondary firing at an elevated temperature as shown in Fig. 3b, c. Further increasing the temperature, however, causes the appearance of large-sized particles and particle aggregation (see Fig. 3d). For LMP-2-*T*, the particles show a tendency to aggregate even if fired at a low temperature (400 °C) without the secondary sintering as seen in Fig. 3e. After being heated at 600 °C for 5 h, the particles show significant growth and aggregation as clearly indicated in Fig. 3f. The smaller particle size and the refrained particle aggregation of LMP-1-*T* originate mainly from its more

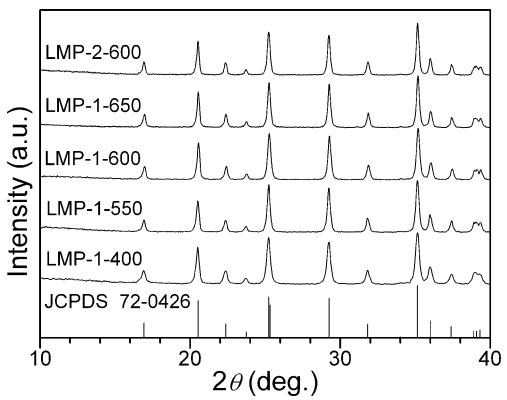

Fig. 2 XRD patterns of $LiMnPO_4$ prepared at different temperatures

homogeneous and smaller-sized precursor. Furthermore, carbon content analyses (see Table 1) show that the LMP-1-*T* samples have higher carbon content than the LMP-2-*T* samples. Clearly, the additional carbon comes from oleic acid. Thermogravimetric analysis showed that oleic acid can be completely pyrolyzed at 400°C [18]. Carbon also exerts an important effect in preventing the growth and aggregation of the particles.

TEM observation was carried out to get an insight into the microstructure of $LiMnPO_4$. Figure 4 gives the typical TEM images of sample LMP-1-600. The particle size ranges from 50 to 150 nm, consistent with the SEM observation as seen in Fig. 4c. A high-resolution TEM (HRTEM) image of an individual $LiMnPO_4$ particle indicates that the particle is coated by a uniform carbon layer with a thickness of around 1–2 nm. Like particle size and distribution, uniform carbon coating is another critical factor in determining the electrochemical performance of the $LiMnPO_4$ material.

Figure 5 shows the charge–discharge curves of samples LMP-1-*T* and LMP-2-*T*. In Fig. 5a, at a current rate of C/20, the first charge capacities of LMP-1-550, LMP-1-600, and LMP-1-650 are 120, 124, and 142 mAh g^{-1}, respectively, while the first discharge capacities of the three samples are 99, 103, and 83 mAh g^{-1}, respectively. It is clear that LMP-1-600 exhibits the best electrochemical performance among the three samples. Therefore, the samples prepared at 600 °C were investigated in the following sections. Figure 5b compares the rate capability between sample LMP-1-600 and LMP-2-600. Note that the reversible capacity of LMP-2-600 at C/20 is only 47 mAh g^{-1}, far below that of LMP-1-600 (103 mAh g^{-1}). At 1-C rate, a reversible capacity of around 60 mAh g^{-1} is still maintained for LMP-1-600, double that for LMP-2-600 at the same rate. The improved electrochemical performance of LMP-1-600 compared with LMP-2-600 can be attributed to its smaller particle size, more uniform size distribution, and higher carbon content.

Co doping was performed to further improve the electrochemical performance of $LiMnPO_4$. Figure 6 gives the XRD patterns of the Co-doped $LiMnPO_4$ (LMP-3-600) with a nominal composition of $LiMn_{0.95}Co_{0.05}PO_4$. The patterns fit well with the $LiMnPO_4$ standard card (JCPDS card no. 72–0426). The lattice parameters calculated from the XRD patterns are shown in Table 2. Note that the substitution of Mn by Co leads to the shrinkage of cell volume since the diameter of Co^{2+} (0.74 Å) is smaller than that of Mn^{2+} (0.8 Å). However, the change in cell volume is minor due to a low level of Co doping. HRTEM observation also confirms that the Co doping results in a minor change in the lattice parameter of the $LiMnPO_4$ crystal. The inset in Fig. 6 shows the SEM image of LMP-3-600; it can be seen that Co doping results in a smaller average particle size and a more uniform size distribution.

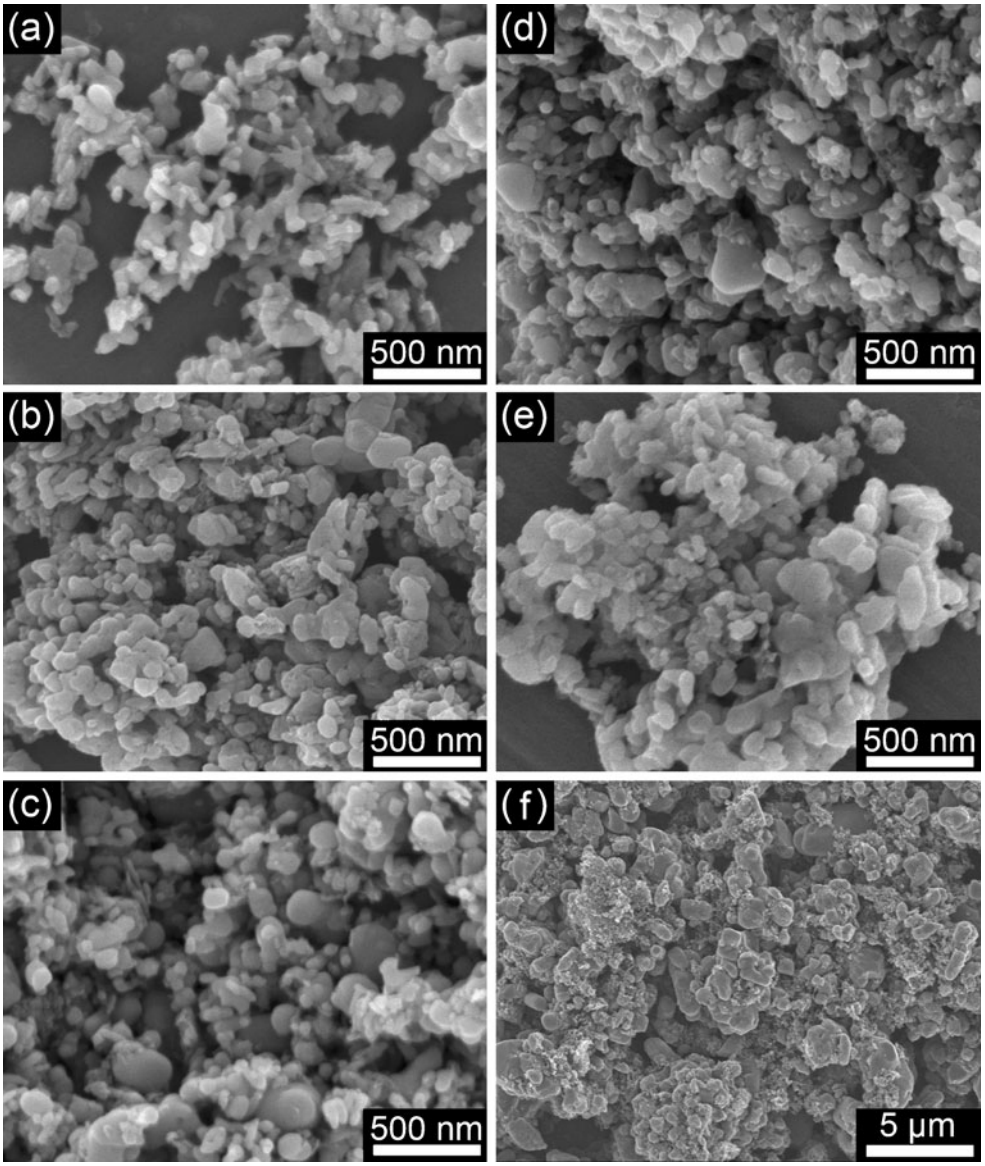

Fig. 3 SEM images of the $LiMnPO_4$ samples: **a** LMP-1-400, **b** LMP-1-550, **c** LMP-1-600, **d** LMP-1-650, **e** LMP-2-400, and **f** LMP-2-600

As expected, Co doping has a minor effect on the carbon content of the sample (3.9 wt.% for LMP-3-600).

Figure 7a shows the charge–discharge curves of LMP-3-600. The first discharge capacities of the sample at 1/20, 1/10, 1/2, and 1 C are 144, 123, 97, and 80 mAh g^{-1}, respectively, greatly higher than those of the undoped sample LMP-1-600. It seems that Co doping activates the $LiMnPO_4$ material, yielding a higher obtainable capacity, which is consistent with the behaviors of other cathodes [29, 30]. Figure 7b compares the cycling stability between LMP-1-600 and LMP-3-600 at different current rates. Note that the LMP-3-600 sample shows a slow capacity fade at C/10, similar to the phenomenon observed in [31].The exact reason for the capacity fade at a low current is unclear yet. At a high current rate, however, the LMP-3-600 sample exhibits a good cycling stability. A good capacity recovery can also be realized when shifted to a low current density for this sample. Since the Co-doped $LiMnPO_4$ has a high

Table 1 Carbon content of the as-prepared $LiMnPO_4$ samples

Samples	LMP-1-400	LMP-1-600	LMP-2-400	LMP-2-600
Carbon content (wt.%)	4.9	3.8	2.7	2.2

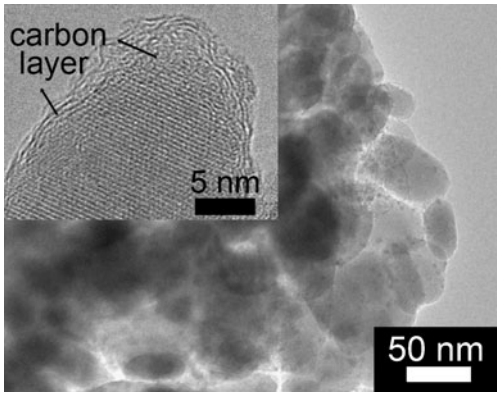

Fig. 4 TEM image of LMP-1-600. The *inset* shows the HRTEM image of an individual particle

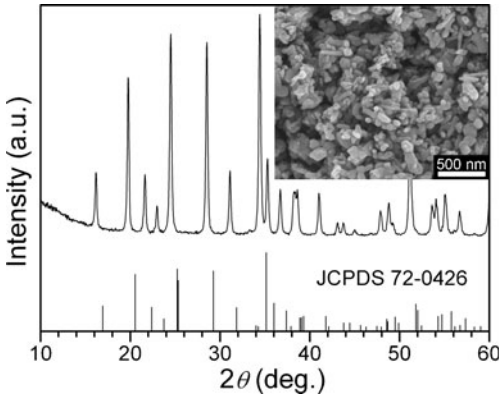

Fig. 6 XRD patterns of LMP-3-600. The *inset* shows the SEM image of LMP-3-600

working voltage and electrochemical performance, it can combine with the high-performance tin-based anodes [32, 33] to make LIBs for potential applications in EV/HEV.

To understand the different electrochemical performance between LMP-1-600 and LMP-3-600, Li-ion chemical diffusion coefficients, $\widetilde{D}_{\mathrm{Li}}$, were measured by the CV method. Figure 8a, b show the CV plots at various scan rates between 2.5 and 5 V. Figure 8c gives the peak current (I_{p}) as a function of square root of the scan rate ($v^{1/2}$) and the corresponding linear fitting. Note that I_{p} exhibits a linear relationship with $v^{1/2}$, which is expected for a diffusion-controlled process. The chemical diffusion coefficients can be calculated with the following equation [34]:

$$I_{\mathrm{P}} = 0.4463\, n^{3/2} F^{3/2} C_{\mathrm{Li}} S R^{-1/2} T^{-1/2} \widetilde{D}_{\mathrm{Li}}{}^{1/2} v^{1/2} \quad (1)$$

where n, F, C_{Li}, S, R, and T represent the charge transfer number, the Faraday constant, the Li-ion concentration (mol cm^{-3}), the surface area of the electrode (cm^2), the gas constant, and the absolute temperature (K), respectively. The $\widetilde{D}_{\mathrm{Li}}$ values in LMP-1-600 and LMP-3-600 are 9.2×10^{-18} and 3.0×10^{-17} cm^2 s^{-1}, respectively. The enhanced diffusion kinetics for LMP-3-600 can be ascribed to the smaller particle size and more homogeneous size distribution, which in turn improved its electrochemical performance. It should be stressed that although the difference in the diffusion coefficients can partly explain the different electrochemical behaviors between the two samples, the exact mechanism, however, should be further explored since the difference in $\widetilde{D}_{\mathrm{Li}}$ values is not significant. Compared to other cathode materials, such as $LiFePO_4$ [34], $LiCoO_2$ [35], and $LiMn_2O_4$ [36], the Li-ion diffusion rate of $LiMnPO_4$ is rather smaller. This can also explain its low affordable capacity even at low current rates.

To further explain the different electrochemical behaviors between LMP-1-600 and LMP-3-600, ac impedance plots were recorded after the cells were cycled for 3 and 60 times as shown in Fig. 9. The Nyquist plots show a semicircle in

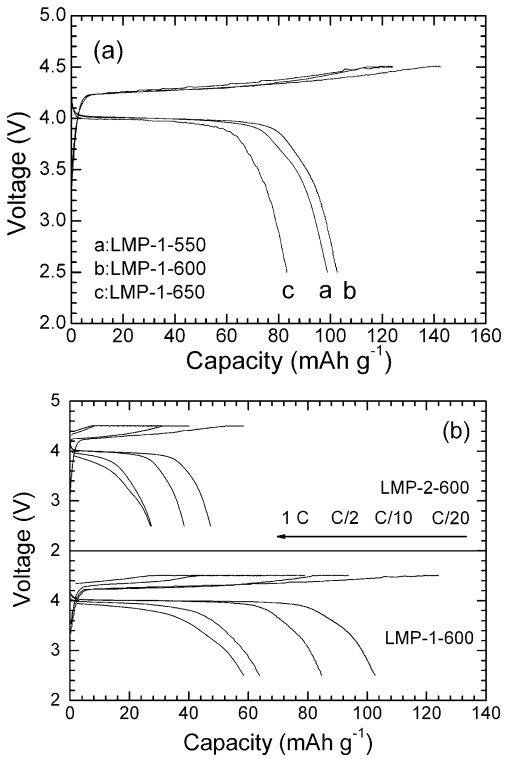

Fig. 5 **a** Charge–discharge curves of LMP-1-T at C/20 and **b** rate capability of LMP-1-600 and LMP-2-600

Table 2 Lattice constants of LMP-1-600 and LMP-2-600

	a (Å)	*b* (Å)	*c* (Å)	*V* (Å^3)
LMP-1-600	6.109	10.461	4.746	303.3
LMP-3-600	6.100	10.445	4.745	302.3

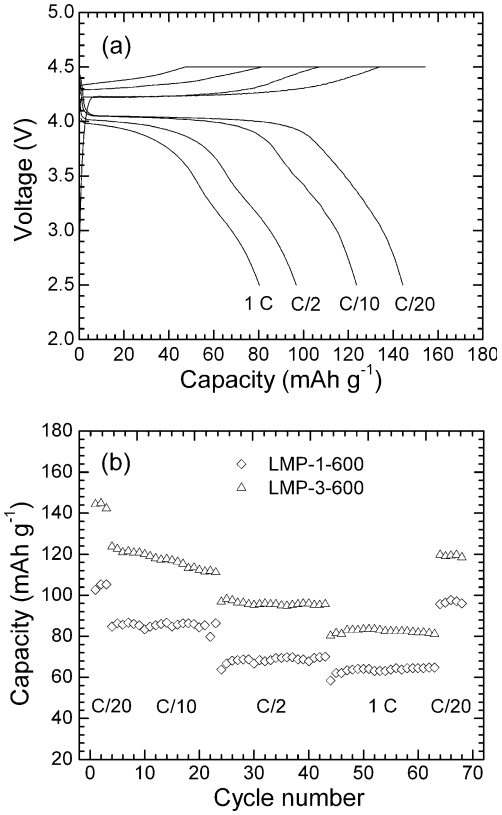

Fig. 7 **a** Rate capability of LMP-3-600 and **b** comparison of cycling stability between LMP-1-600 and LMP-3-600

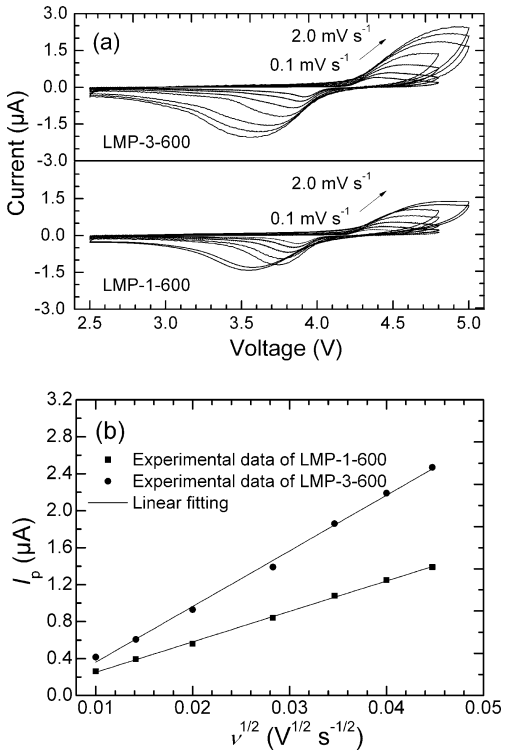

Fig. 8 **a** CV plots of LMP-1-600 and LMP-3-600 at various scan rates and **b** peak current I_p as a function of square root of scan rate $\nu^{1/2}$ and the corresponding linear fitting

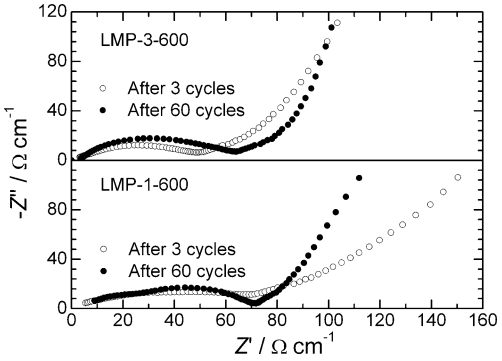

Fig. 9 Impedance plots of the LMP-3-600 and LMP-1-600electrodes after 3 and 60 cycles

the high frequency region and a slopping line in the low frequency region. As is well established, the semicircle is related to the charge transfer resistance (R_{ct}), while the sloping line is referred to the Warburg impedance, corresponding to the Li-ions diffusion in the bulk electrode. Note that the LMP-3-600 electrode demonstrates a smaller R_{ct} than LMP-1-600 both after 3 and after 60 cycles, indicating the faster diffusion of Li-ions across the LMP-3-600/electrolyte interface than across the LMP-1-600/electrolyte interface. The faster interfacial diffusion for LMP-3-600 is due to its smaller particle size (with a large specific surface area) that maximizes the contact with the electrolyte. It should be noted that for both electrodes, an increase in R_{ct} is observed upon repeated cycling, which can explain their poor electrochemical performance after long-term cycling. Again, the EIS results can only partly explain the different electrochemical behaviors since the difference in EIS is not remarkable.

Conclusions

Nanosized $LiMnPO_4$ powders were successfully prepared by oleic acid-assisted solid-state reaction. The introduction of oleic acid during ball milling leads to the small size and uniform distribution of the precursors, resulting in optimized morphology and improved electrochemical performance of the final products. The sample prepared at 600°C using an oleic acid-treated precursor exhibits the best electrochemical performance, delivering discharge capacities of 103 and 58 mAh g^{-1} at 1/20 and 1 C, respectively. Co doping further improves the electrochemical performance. The discharge capacities of the Co-doped sample reach 144 and 80 mAh g^{-1} at t 1/20 and 1 C, respectively, far higher than those of the undoped sample. The enhancement of the electrochemical performance can be attributed to the reduced particle size and optimized size distribution by Co doping that facilitates the Li-ion

diffusion in bulk electrode and the diffusion through the electrode/electrolyte interface.

Acknowledgments This work was supported by Zijin Program of Zhejiang University, China, the Fundamental Research Funds for the Central Universities (No. 2010QNA4003), the Ph.D. Programs Foundation of Ministry of Education of China (No. 20100101120024), and the Foundation of Education Office of Zhejiang Province (No. Y201016484).

References

1. Brodd RJ, Bullock KR, Leising RA, Middaugh RL, Miller JR, Takeuchi E (2004) Batteries, 1977 to 2002. J Electrochem Soc 151:K1–K11
2. Aricò AS, Bruce P, Scrosati B, Tarascon JM, Schalkwijk WV (2005) Nanostructured materials for advanced energy conversion and storage devices. Nat Mater 4:366–377
3. Horiba T, Maeshima T, Matsumura T, Koseki M, Arai J, Muranaka Y (2005) Applications of high power density lithium ion batteries. J Power Sources 146:107–110
4. Wu XL, Jiang LY, Cao FF, Guo YG, Wan LJ (2009) $LiFePO_4$ nanoparticles embedded in a nanoporous carbon matrix: superior cathode material for electrochemical energy-storage devices. Adv Mater 21:2710–2714
5. Cao H, Xia BJ, Zhang Y, Xu NX (2005) $LiAlO_2$-coated $LiCoO_2$ as cathode material for lithium ion batteries. Solid State Ionics 176:911–914
6. Chen ZH, Qin Y, Amine K, Sun YK (2010) Role of surface coating on cathode materials for lithium-ion batteries. J Mater Chem 20:7606–7612
7. Luo WB, Li XH, Dahn JR (2010) Synthesis and characterization of Mg substituted $LiCoO_2$. J Electrochem Soc 157:782–790
8. Padhi AK, Nanjundaswamy KS, Goodenough JB (1997) Phospho-olivines as positive-electrode materials for rechargeable lithium batteries. J Electrochem Soc 144:1188–1194
9. Li GH, Azuma H, Tohda M (2002) $LiMnPO_4$ as the cathode for lithium batteries. Electrochem Solid-State Lett 5:A135–A137
10. Bramnik NN, Bramnik KG, Buhrmester T, Baehtz C, Ehrenberg H, Fuess H (2004) Electrochemical and structural study of $LiCoPO_4$-based electrodes. J Solid State Electrochem 8:558–564
11. Wolfenstine J, Allen J (2004) $LiNiPO_4$–$LiCoPO_4$ solid solutions as cathodes. J Power Sources 136:150–153
12. Son CG, Yang HM, Lee GW, Cho AR, Aravindan V, Kim HS, Kim WS, Lee YS (2011) Manipulation of adipic acid application on the electrochemical properties of $LiFePO_4$ at high rate performance. J Alloys Compd 509:1279–1284
13. Zaghib K, Dontigny M, Guerfi A, Charest P, Rodrigues I, Mauger A, Julien CM (2011) Safe and fast-charging Li-ion battery with long shelf life for power applications. J Power Sources 196:3949–3954
14. Kang B, Ceder G (2009) Battery materials for ultrafast charging and discharging. Nature 458:190–193
15. Jin B, Gu HB, Kim KW (2008) Effect of different conductive additives on charge/discharge properties of $LiCoPO_4$/Li batteries. J Solid State Electrochem 12:105–111
16. Wang F, Yang J, NuLi Y, Wang JL (2010) Highly promoted electrochemical performance of 5V $LiCoPO_4$ cathode material by addition of vanadium. J Power Sources 195:6884–6887
17. Wolfenstine J, Allen J (2005) Ni^{3+}/Ni^{2+} redox potential in $LiNiPO_4$. J Power Sources 142:389–390
18. Choi D, Wang D, Bae IT, Xiao J, Nie Z, Wang W, Viswanathan VV, Lee YJ, Zhang JG, Graff GL, Yang Z, Liu J (2010) $LiMnPO_4$ nanoplate grown via solid-state reaction in molten hydrocarbon for Li-ion battery cathode. Nano Lett 10:2799–2805
19. Kavan L, Bacsa R, Tunckol M, Serp P, Zakeeruddin SM, Formal FL, Zukalova M, Graetzel M (2010) Multi-walled carbon nanotubes functionalized by carboxylic groups: activation of TiO_2 (anatase) and phosphate olivines ($LiMnPO_4$; $LiFePO_4$) for electrochemical Li-storage. J Power Sources 195:5360–5369
20. Lee JW, Park MS, Anass B, Park JH, Paik MS, Doo SG (2010) Electrochemical lithiation and delithiation of $LiMnPO_4$: effect of cation substitution. Electrochim Acta 55:4162–4169
21. Wang D, Ouyang C, Drézen T, Exnar I, Kay A, Kwon NH, Gouerec P, Miners JH, Wang M, Grätzel M (2010) Improving the electrochemical activity of $LiMnPO_4$ via Mn-site substitution. J Electrochem Soc 157:A225–A229
22. Bakenov Z, Taniguchi I (2010) $LiMg_xMn_{1-x}PO_4$/C cathodes for lithium batteries prepared by a combination of spray pyrolysis with wet ball milling. J Electrochem Soc 157:A430–A436
23. Yao J, Bewlay S, Konstantionv K, Drozd VA, Liu RS, Wang XL, Liu HK, Wang GX (2006) Characterisation of olivine-type $LiMn_xFe_{1-x}PO_4$ cathode materials. J Alloys Compd 425:362–366
24. Wang D, Buqa H, Crouzet M, Deghenghi G, Drezen T, Exnar I, Kwon NH, Miners JH, Poletto L, Grätzel M (2009) High-performance, nano-structured $LiMnPO_4$ synthesized via a polyol method. J Power Sources 189:624–628
25. Bramnik NN, Ehrenberg H (2008) Precursor-based synthesis and electrochemical performance of $LiMnPO_4$. J Alloys Compd 464:259–264
26. Bakenov Z, Taniguchi I (2010) Physical and electrochemical properties of $LiMnPO_4$/C composite cathode prepared with different conductive carbons. J Power Sources 195:7445–7451
27. Bakenov Z, Taniguchi I (2010) Electrochemical performance of nanocomposite $LiMnPO_4$/C cathode materials for lithium batteries. Electrochem Commun 12:75–78
28. Oh SM, Oh SW, Myung ST, Lee SM, Sun YK (2010) The effects of calcination temperature on the electrochemical performance of $LiMnPO_4$ prepared by ultrasonic spray pyrolysis. J Alloys Compd 506:372–376
29. Alcántara R, Ortiz G, Tirado JL, Stoyanova R, Zhecheva E, Ivanovab S (2009) Fe^{3+} and Ni^{3+} impurity distribution and electrochemical performance of $LiCoO_2$ electrode materials for lithium ion batteries. J Power Sources 194:494–501
30. Alcántara R, Ortiz GF, Lavela P, Tirado JL, Jaegermann W, Thißen A (2005) Rotor blade grinding and re-annealing of $LiCoO_2$: SEM, XPS, EIS and electrochemical study. J Electroanal Chem 584:147–156
31. Yang G, Ni H, Liu H, Gao P, Ji H, Roy S, Pinto J, Jiang X (2011) The doping effect on the crystal structure and electrochemical properties of $LiM_xM_{1-x}PO_4$ (M=Mg, V, Fe, Co, Gd). J Power Sources 196:4747–4755
32. Ortiz GF, Hanzu I, Lavela P, Knauth P, Tirado JL, Djenizian T (2010) Nanoarchitectured TiO_2/SnO: a future negative electrode for high power density Li-ion microbatteries. Chem Mater 22:1926–1932
33. Ortiz GF, Hanzu I, Knauth P, Lavela P, Tirado JL, Djenizian T (2009) Nanocomposite electrode for Li-ion microbatteries based on SnO on nanotubular titania matrix. Electrochem Solid-State Lett 12:186–189
34. Xie J, Imanishi N, Zhang T, Hirano A, Takeda Y, Yamamoto O (2009) Li-ion diffusion kinetics in $LiFePO_4$ thin film prepared by radio frequency magnetron sputtering. Electrochim Acta 54:4631–4637
35. Xie J, Imanishi N, Hirano A, Matsumura M, Takeda Y, Yamamoto O (2007) Kinetics investigation of a preferential (104) plane oriented $LiCoO_2$ thin film prepared by RF magnetron sputtering. Solid State Ionics 178:1218–1224
36. Wu XM, He ZQ, Chen S, Ma MY, Xiao ZB, Liu JB (2007) The effect of thickness on the properties of solution-deposited $LiMn_2O_4$ thin films. Mater Chem Phys 105:58–61